Layer-by-layer (LbL) assembly of polyelectrolytes at the surface of a fiberglass membrane used as a support of the polarized liquid–liquid interface

Borgul, Paulina; Rudnicki, Konrad; Chu, Liangyong; Leniart, Andrzej; Skrzypek, Sławomira; Sudhölter, Ernst J.R.; Poltorak, Lukasz

DOI
10.1016/j.electacta.2020.137215

Publication date
2020

Document Version
Accepted author manuscript

Published in
Electrochimica Acta

Citation (APA)
Borgul, P., Rudnicki, K., Chu, L., Leniart, A., Skrzypek, S., Sudhölter, E. J. R., & Poltorak, L. (2020). Layer-by-layer (LbL) assembly of polyelectrolytes at the surface of a fiberglass membrane used as a support of the polarized liquid–liquid interface. *Electrochimica Acta*, *363*, Article 137215. https://doi.org/10.1016/j.electacta.2020.137215

Layer-by-layer (LbL) assembly of polyelectrolytes at the surface of a fiberglass membrane used as a support of the polarized liquid-liquid interface

Paulina Borgul,[a] Konrad Rudnicki,[a] Liangyong Chu,[b] Andrzej Leniart,[a] Sławomira Skrzypek,[a] Ernst J. R. Sudhölter,[c] Lukasz Poltorak*[a]

a. Department of Inorganic and Analytical Chemistry, Electroanalysis and Electrochemistry Group, Faculty of Chemistry, University of Lodz, Tamka 12, 91-403 Lodz, Poland.
b. Department of Mechanics of Solids, Surfaces&Systems (MS3), University of Twente, Drienerlolaan 5, 7500 AE Enschede, The Netherlands.
c. Delft University of Technology, Department of Chemical Engineering, Van der Maasweg 9, 2629 HZ Delft, The Netherlands.

***Corresponding author:** Lukasz.poltorak@chemia.uni.lodz.pl

In this work, the electrified liquid-liquid interface (LLI) was supported with the bare and polyelectrolyte modified fiberglass membranes. The permeability of these supports was then investigated with ion transfer voltammetry. This work descends from three mutually interconnected experimental tasks. (i) The study of an interfacial behavior of three polyelectrolytes, poly(ethyleneimine) (PEI), polystyrene sulfonate (PSS), and polyhexamethylene guanidine (PHMG) at the polarized LLI. (ii) Electrochemical characterization of the LLI supported by the unmodified fiberglass membrane. (iii) Polyelectrolyte multilayer placement, using layer-by-layer processing, at the surface of the fiberglass membrane and its further utilization as the support for the electrified LLI. Bare and modified membranes were characterized using ion transfer voltammetry in the presence of a family of quaternary ammonium cations: tetramethylammonium (TMA^+), tetraethylammonium (TEA^+), tetrapropylammonium ($TPrA^+$) and tetrabutylammonium (TBA^+) initially dissolved in the aqueous phase as the chloride salts. The ionic currents related to their transmembrane transfer were affected already after the first polyelectrolyte layer placement. In addition to electrochemistry, the modification process was followed using several

complementary techniques, including optical microscopy, atomic force microscopy, infra-red spectroscopy, and scanning electron microscopy. The proposed methodology offers very simple, fast, and versatile (having in mind the available selection of functional polyelectrolytes) protocol for a membrane preparation having size sieving properties. In turn, the electrochemistry at the liquid-liquid interface can be used as an insightful tool to study the ionic transmembrane currents.

1.1. Introduction

Surface modification protocols based on an alternating placement of an oppositely charged deposit aliquots, known as the layer-by-layer (LbL) assembly, is an immensely and increasingly popular technique for nanofilms formation. This is mainly due to the unbelievably simple processing, especially when it comes to direct deposition from a solution. The materials that may be used in this respect cover DNA, proteins including enzymes, nano- and micro-particles, self-assembled phospholipids, and finally polymers [1,2]. The latter is usually represented by polyelectrolytes equipped with permanently or ionizable chemical functional groups such as primary, secondary, tertiary, and quaternary ammonium cations (e.g. polyallylamine or poly(diallyldimethylammonium chloride), sulfonate (e.g. polystyrene sulfonate) or carboxylate anions (e.g. polyvinyl acetate). Multilayer films made out of charged polyelectrolytes make an impressive list of applications. Placement of enzymes into polyelectrolyte multilayer is a popular approach during biosensors [3,4] or biocatalytic surfaces [5–7] construction. Soft and charged polymeric deposits can serve as a cushion with a switchable surface charge for lipid bilayers based bio-interphases development [8–12]. Polyelectrolyte capsules derived from LbL processing are used as active substance carriers [13–15], whereas polyelectrolyte based coatings at the surface of nano- or micro-particles find applications in molecular recovery [16]. The decoration of membranes with polyelectrolyte multilayer gathered significant attention in recent years as these molecules bring new functional properties to the membrane interfacial region. Numerous reports prove that chosen polyelectrolytes present at the membranes surface exhibit antifouling properties [17–19]. The polyelectrolyte multilayer may induce the selective transport of

ions across the membrane [20–23] or even tune the ionic flux by careful adjustment of the terminating layer charge [24]. Finally, the properties of a chemical functional group(s) located within the polyelectrolyte structure can give a membrane the functional properties as e.g. membranes modified with guanidine group containing polyelectrolyte for phosphate recovery applications [25,26]. With the wide selection of polyelectrolytes tailored by synthetic chemistry toolbox (allowing for programmed chemical properties) and modifier thickness controlled by a very simple LbL assembly, the concerned method deserves to be considered as one of the most powerful among surface modification strategies.

Liquid-liquid interface (LLI) forms a soft boundary that can be crossed by the chemical species fulfilling inherent partitioning properties. In other words, the transfer of chemical species will proceed towards the phase of their highest affinity until equilibrium will be established. Under certain circumstances, this is at the interface between two immiscible electrolyte solutions (ITIES), electrochemistry can be used to disturb this equilibrium [27,28]. Interfacial polarization may lead to a selective transfer of ionic species from the aqueous to the organic phase or from the organic to the aqueous phase as the standard Galvani potential of ion transfer is directly related to the standard Gibbs free energy of the ion transfer reaction ($\Delta G^0_{i,aq\leftrightarrow org} = -z_i F \Delta^{aq}_{org}\phi^0_{i,aq\leftrightarrow org}$). This simply means that the portion of energy supplied to a biphasic system (potential difference applied from an external power source) needed to trigger simple interfacial ion transfer is directly related to molecular hydrophilicity/hydrophobicity. Moreover this soft junction is self-healing, impossible to scratch and under proper composition of both contacting phases can be studied with a full range of available electrochemical techniques. Desired (and new) physical and chemical properties of the LLI can be easily introduced with the help of interfacial modification [29]. In this respect, the interfacial ionic currents can be affected by two means. The first one relays on the placement of the physical obstacles in a form of molecular layers [30,31] or solid particles [32] self-assembling at the LLI. With a wide choice of chemical functional groups present at the surface of the self-assembling objects (e.g. phospholipid polar head groups, reach chemistry of nanoparticles), these are readily available building

blocks that can be easily placed at the soft junctions. The second approach is based on membranes with predefined dimensionality [33–36] and/or geometrical arrangement [37–39] of pores that are used as the LLI supports. When the diameter of a single pore approaches few tens of micrometers the higher mass transfer coefficients of the chemical species crossing the interface are obtained due to a transition from a linear to hemispherical diffusion zones established at the ingress of the pore(s). This finds applications in sensing [40] and maybe harvested in molecular separation [41]. Further pore(s) downscaling, for instance in mesoporous membranes, will eventually reach the dimensions of macro- and small molecules giving elegant platforms for molecular sieving [34,42–44]. In this respect, the electrochemistry at the LLI provides direct tools to investigate the ionic currents flowing through the interface situate within the membrane pore(s).

In this work, we have combined the very simple LbL assembly of polyelectrolytes at the surface of a fiberglass membrane that was further used as a support for the electrified LLI. The family of the quaternary ammonium cations, including tetramethylammonium, tetraethylammonium, tetrapropylammonium, and tetrabutylammonium, were used to study the permeability of the bare and polyelectrolyte multilayer modified fiberglass membrane. Our findings indicate that each layer placed at the membrane surface affected the ionic currents and energetics of the studied interfacial ion transfer reactions as followed by the ion transfer voltammetry (ITV). Reported results indicate that the controlled thickness of the polyelectrolyte multilayer may be used for constructing the membrane with the desired size sieving properties.

1.2. Methods and Materials

1.2.1. Materials

Sodium chloride (NaCl, for analysis, ChemPur), hydrochloric acid (HCl, 35 – 38% vol, for analysis, ChemPur), sodium hydroxide (NaOH, for analysis, ChemPur), 1,2-dichloroethane (1,2-DCE, for analysis, POCH), poly(ethyleneimine) (PEI, M.W. 25k, Sigma-Aldrich), polystyrene sulfonate (PSS, M.W. 70k, Sigma-Aldrich) and polyhexamethylene guanidine (PHMG, >99%, Sinotech),

tetramethylammonium chloride (TMACl, >98%, Acros Organics), tetraethylammonium chloride (TEACl, >99%, Alfa Aesar), tetrapropylammonium chloride (TPrACl, >99%, Alfa Aesar), tetrabutylammonium (TBACl, 97%, Apollo Scientific) were all used as received. Potassium tetrakis(4-chlorophenyl)borate (KTPBCl, ≥98%, Sigma-Aldrich) and bis(triphenylphosphoranylidene)ammonium chloride (BTPPACl, 97%, Sigma-Aldrich) were mixed after dissolving the equimolar amounts in methanol (MeOH, for analysis, ChemPur) and water mixture (1:2 by volume). Resulting precipitate, bis(triphenylphosphoranylidene)ammonium tetrakis(4-chlorophenyl)borate (BTPPATPBCl) was filtrated, dried and recrystallized from acetone. Before electrochemical measurement and modification fiberglass membranes (Glass microfiber discs by Ahlstrom Munksjo, diameter = 47.0 mm, 0.2 mm thick) were cut using scalpel knife and attached to the glass tubing (internal diameter = 6.0 mm, outer diameter = 9.0 mm, length = 50.0 mm) using silicon sealant (Diall, Kingfisher Int. UK).

1.2.2. Electrochemical cells

All electrochemical experiments described in this work were performed in two electrochemical cells shown in Fig. 1A and 1B. LLI was polarized with the help of a four-electrode configuration with two platinum wires used as the counter electrodes and two Ag/AgCl wires used as the reference electrodes. Each phase contained one platinum and one Ag/AgCl electrode (see Fig. 1A and 1B for the arrangement of the electrodes). The potential was supplied from an external power source using potentiostat-galvanostat Autolab 302N from Methrom. The interfacial behavior of the polyelectrolytes used as the fiberglass membrane modifiers were studied in the cell shown in Fig. 1A that can be additionally depicted as:

$$Ag|AgCl|\,{}^{10\ mM\ NaCl}_{x\ mg/mL\ polyelectrolyte}\,\Big|\Big|\,{}^{5\ mM}_{BTPPATPBCl}\Big|\,{}^{10\ mM\ NaCl}_{10\ mM\ BTPPACl}\,|AgCl|Ag \qquad \text{Cell I}$$

$$Ag|AgCl|\,{}^{10\ mM\ NaCl,\ 10\ mM\ H_3PO_4,}_{x\ mL\ 1\ M\ NaOH, x\ \mu g/mL\ PHMG}\,\Big|\Big|\,{}^{5\ mM}_{BTPPATPBCl}\Big|\,{}^{10\ mM\ NaCl}_{10\ mM\ BTPPACl}\,|AgCl|Ag \qquad \text{Cell II}$$

----------Here Figure 1----------

The modified (Fig. 1D) and unmodified (Fig. 1C – optical microscopy photo) fiberglass membranes were studied in the cell shown in Fig. 1B. Before electrochemical characterization, the membranes were fixed to a glass tube (internal diameter = 8 mm; external diameter = 10 mm) using a silicone sealant. Next, the tube was filled with the organic phase and was further placed into a glass cell containing the aqueous phase. Finally, all electrodes were inserted. The organic phase reference electrode was additionally placed inside the capillary filled with the aqueous solution of 10 mM BTPPACl and 10 mM NaCl. The electrochemical cell can be represented by (TAA^+ stands for tetraalkylammonium (TMA^+,TEA^+,$TPrA^+$ or TBA^+) cation):

$$Ag|AgCl|\begin{matrix}10\ mM\ NaCl\\ x\ \mu M\ TAA^+\end{matrix}\Big|\Big|\begin{matrix}5\ mM\\ BTPPATPBCl\end{matrix}\Big|\begin{matrix}10\ mM\ NaCl\\ 10\ mM\ BTPPACl\end{matrix}|AgCl|Ag \qquad \text{Cell III}$$

1.2.3. Infra-red spectroscopy

The fiberglass membrane modified with PEI followed by 5 (PSS-PHMG) layers placement was dried and pounded in a mortar. The same was done for the unmodified membrane. Next, the powder was dispersed in the KBr, and the pellet was formed. The spectra were recorded using Nexus FT-IR (Thermo Nicolet) spectrometer in a spectral window from 4000 cm^{-1} to 2000 cm^{-1}.

1.2.4. Scanning Electron Microscopy

The scanning electron microscopy (SEM, a Phenom G2 Pure, FEI Company, the Netherlands) was used to imagine fiberglass membranes before and after the modification process. During the measurements, the fiberglass membranes were fixed to a SEM support with copper tape. SEM images were acquired using a high sensitivity backscatter electron detector (BSD) with an accelerating voltage of 5 kV.

1.2.5. Atomic Force Microscopy

The atomic force microscopy (AFM) morphology characterization is performed using a Park XE-100 AFM from Park Systems using an ACTA AFM probe purchased from AppNano. The spring constant

of the probe is 26 N/m determined using the thermal noise method [45,46]. The surface roughness of individual fibers is calculated using the XEI software from Park systems.

1.3. Results and discussion

1.3.1. Behavior of polyelectrolytes at the polarized liquid-liquid interface

Before fiberglass membrane modification, the interfacial behavior of PEI, PSS, and PHMG was studied at the electrified LLI in the electrochemical cell shown in Fig. 1A. Fig. 2 represents the ion transfer voltammograms recorded in the cell I for x = 50 $\mu g \cdot mL^{-1}$. The pH of the 10 mM NaCl usually found in the range from 5.5 (caused by the carbon dioxide dissolution) to 7 assures positive charge of PEI (for branched species the pK_a values falls for the range from 8 to 11) [47] and PHMG (pK_a = 13.5) [48]. At given pH PSS will be fully dissociated ($pK_a \approx 1$) [49] and negatively charged. Since only charged chemical species can give a signal at the electrified LLI, under the present experimental conditions all three macromolecules are expected to give a signal. However, only the addition of PEI and PHMG to the water phase resulted in the appearance of a pair of asymmetric peaks on the positive side of the potential window (Fig. 2A and 2B).

----------Here Figure 2----------

These voltammograms share a series of similar electrochemical characteristics common for the interfacially active and charged macromolecules. These include (i) irregular shape of the peaks; (ii) forward and reverse peak charge ratio diverging from unity; (ii) sudden drops in peak currents especially recorded on the reverse scan (in case of PEI and PHMG recorded during polarization from higher to lower potential values); (iv) peak to peak separation deviating from the expected value defined by the molecular charge ($\Delta Ep = \frac{0.059\,V}{z}$, where z is the molecular charge) and (v) the increase in the capacitive currents upon repetitive cycling (data not shown) that are commonly found for the molecules adsorbing to the LLI. The mechanism behind the recorded charge transfer reaction is common for all macromolecules [50–55] and involves a few steps. Most reports deal with the positively charged macromolecules initially dissolved in the aqueous phase, which we also focus on in

our considerations. In the first step, the interfacial polarization with the direction from the lower to the higher potential values triggers the transfer of the positively charged polyelectrolytes from the bulk phase to the LLI region where the accumulation of the positive charge occurs. This, in turn, facilitates the interfacial transfer of the hydrophobic anion from the organic phase background electrolyte to the water phase where it can form a complex with the positively charged macromolecule [56]. This reaction can be directly probed by ITV as it gives positive currents observed for PEI (Fig. 2A) and PHMG (Fig. 2B). On the vertex potential, the direction of polarization is changed and the negative currents are recorded as the hydrophobic anions are returning to the organic phase. After reaching the maximum negative peak height the current is dropping in an abrupt manner indicating the interfacial adsorption process. During consecutive voltammetric cycling, the hydrophobic anion – positively charged macromolecule complexes precipitate at the electrified LLI and form molecular films visible with the naked eye [52,53]. The voltammogram showed in Fig. 2C was recorded in the presence of 50 μg·mL^{-1} PSS in the aqueous phase and is the same as the blank voltammogram showed in Fig. 2D recorded at the LLI formed between 10 mM NaCl in the aqueous phase and 5 mM BTPPATPBCl in the organic phase. For the negatively charged polyelectrolyte, we would expect to observe the appearance of a signal within the less positive potential range due to the facilitated transfer of the hydrophobic cation present in the organic phase. Since this was not the case, under the configuration studied, the presence of PSS in the water phase cannot be followed using ITV and we attributed the faradaic currents limiting the potential window on the less positive potential side (for both, Fig. 2C and 2D) to the transfer of $Cl^-_{aq\leftrightarrow org}$.

Next, we focused on understanding the interfacial behavior of PHMG (PEI was already comprehensively studied by Ulmeanu *et al.* [55] whereas PSS is electrochemically inactive). The positive peak current attributed to the PHMG added to the aqueous phase could be detected from concentrations equal to 8 μg·mL^{-1} and increased linearly up to 50 μg·mL^{-1} (see Fig. SI1 from supporting information). Also, we found that the positive peak currents – corresponding to the transfer of the TPBCl$^-$ from the organic phase to the aqueous phase – increased linearly with the square root of the

scan rate (see Fig. SI2 from supporting information) which is typical behavior of a diffusion-limited process. Fig. 3 and Fig. SI3 show that PHMG is interfacially active in almost the entire conventional pH scale (studied in cell II), at least up to the last studied pH value equal to 12.0, agreeing with its pK_a = 13.5. We also found that the positive and negative signal intensities change upon repetitive voltammetric cycling (Fig. 3A) giving pH-dependent patterns shown in Fig. 3B. As we change the pH, we also change the form of phosphate species that were used to buffer the aqueous phase, this is $H_2PO_4^-$ at pH = 5.0; ≈ 1:1 mixture of $H_2PO_4^-$ and HPO_4^{2-} at pH = 7.4; HPO_4^{2-} at pH = 10.0 and ≈1:1 mixture of PO_4^{3-} and HPO_4^{2-} at pH = 12.0. The current – ITV repetition number patterns from Fig. 3B can be explained based on the guanidine group present in the PHMG structure interactions with the phosphate species [25,57]. These are based on the electrostatic attraction between oppositely charged ions and the ability to form hydrogen bonding, especially for the protonated phosphate species existing at pH < 12.0. The positive peak current drop recorded after 100 voltammetric cycles from Fig. 3B equals to around 6%; 23%; 42% and 48% for pH = 12.0; 10.0; 7.4 and 5.0, respectively. This dependency indicates that the phosphate species from the aqueous phase most probably compete with the $TPBCl^-$ from the organic phase during interfacial complexation reaction with positively charged polyelectrolyte. The highest drop in the positive peak current for pH 5.0 and 7.4 is not surprising as the protonated phosphate species, in addition to the electrostatic interactions, can form the hydrogen bonding with the guanidine group. At higher pH values, especially at pH = 12.0, the change in the recorded current upon repetitive cycling is negligible indicating that the electrostatic and hydrophobic interactions between positively charged polyelectrolyte and the $TPBCl^-$ are stronger than only electrostatic interactions with PO_4^{3-}. PEI, PHMG, and PSS were further used for the polyelectrolyte multilayer formation at the surface of a fiberglass membrane.

----------Here Figure 3----------

1.3.2. Polarized liquid-liquid interface supported with the fiberglass membrane

The unmodified fiberglass membranes were studied as the support of the electrified LLI. Before measurements, each membrane underwent similar processing involving a few steps. (i) First, the membrane was fixed to a glass tube using a silicone sealant. (ii) Next, its surface was activated by immersing the membrane in 1M NaOH for a few seconds followed by (iii) thorough rinsing in distilled water. (iv) Following that, the organic phase was added to the tube (v) which was then placed into a glass cell containing the aqueous phase – shown in Fig. 1B.

----------Here Figure 4----------

Fig. 4A shows the ion transfer voltammogram recorded in cell III in the absence (black curve) and the presence (red curve) of TMA^+ initially present in the aqueous phase at a concentration equal to 150 µM. Addition of TMA^+ resulted in an appearance of the signal at around 0.65 V. The forward positive peak current (recorded during interfacial polarization with direction from lower to higher potential values) is due to the TMA^+ transfer from the aqueous to the organic phase, whereas the negative peak current is recorded on the TMA^+ back transfer from the organic to the aqueous phase. From the shape and the electrochemical characteristics provided by the voltammograms from Fig. 4A we can extract a few interesting findings that are based on the assumption that the pores within the membrane are fully wetted by the aqueous phase. First of all, the sigmoidal shape of the forward and reversed peak currents attributed to the TMA^+ indicate that the mass transfer of the charge crossing the interface is enhanced (at least partially). This is a characteristic behavior of LLI placed within the miniaturized pore(s) located in a thin film where the mass transfer of the interfacially active species is governed by the hemispherical diffusion zones established on both sides of the LLI [58]. Having in mind that fiberglass membrane is made out of pressed glass fibers the resulting pores available within its framework will have different shapes and random arrangement – as we schematically show in Fig. 4B. This also means, that some of the pores will be equipped with the individual, whereas other neighboring pores will be sharing the diffusion zones. For our further considerations, we will simplify our system and assume that most of the pores are circular (with r = 0.5 µm assumed based on the

membrane specification) and sufficiently separated from each other. Like so, we can estimate the electroactive surface area of an electrified LLI using the following expression:

$$I_{SS} = 4NrnFDC \qquad \text{eq. 1}$$

where I_{SS} is the steady state current of the $TMA^{+}_{aq \rightarrow org}$ (3.85 µA); n is the charge of TMA^{+} (z = 1), D is the diffusion coefficient of TMA^{+} ($13.8 \cdot 10^{-6}$ $cm^2 \cdot s^{-1}$), C is the TMA^{+} concentration (150 µM), r is the pore radii (assumed to be equal to 0.5 µm) and N is the number of pores located within the membrane. The simple calculations allow for the number of pores (N) estimation which is equal to around $9.6 \cdot 10^4$. With $7.9 \cdot 10^{-9}$ cm^2 as the surface area of a single pore, we get $7.6 \cdot 10^{-4}$ cm^2 as the total electrochemical surface area. This is only a small fraction of a geometrical area of a membrane equal to 0.6 cm^2. Fig. 5 shows a series of ion transfer voltammograms for TMA^{+} (Fig. 5A), TEA^{+} (Fig. 5C), $TPrA^{+}$ (Fig. 5E) and TBA^{+} (Fig. 5G) recorded at 50; 100; 150 and 200 µM concentrations. The unmodified membranes are permeable to all studied cations (the transfer of TBA^{+} shown in Fig. 5G, although overlaid with the potential window limiting current is still present). The shape of the signals recorded during the forward and reversed ion transfer reaction – sigmoidal waves rather than peaks – can be noticed for three smallest ions studied. Also, the successive addition of the studied ions to the electrochemical cell caused the signals to increase in a manner shown in Fig. 5B, 5D, 5F, and 5H. Senthilkumar *et al.* have shown that the diffusion coefficients of TEA^{+} within a compact membrane made out of zeolite Y placed at the electrified LLI are two orders of magnitude lower than corresponding bulk values. To see if the fiberglass membranes used in this work affect the diffusivity of ionic species crossing the LLI located within its pores we correlate the slope of the experimental current – concentration dependencies with the theoretical values (see Fig. SI4A and SI4B). These in turn were calculated based on eq. 1, using previously calculated $9.6 \cdot 10^4$ as the number of pores within the membrane and 0.5 µm being the average pore radii. The diffusion coefficients of TMA^{+}, TEA^{+}, $TPrA^{+,}$ and TBA^{+} were taken from the literature and equal to $13.80 \cdot 10^{-6}$; $10.00 \cdot 10^{-6}$; $6.99 \cdot 10^{-6}$ and $6.35 \cdot 10^{-6}$ $cm^2 s^{-1}$ [59]. As shown in Fig. SI4B, the slopes of the experimental current – concentration dependences nicely correlated with theoretical

values (slope was 1.2) meaning that all species can freely diffuse through the LLI supported with the fiberglass membrane. Also, it was found that the modified LLI interface provides a slightly elongated potential window (interfacial transfer of the background electrolyte ions is affected) and higher resistance as compared with the bare system (see Fig. SI5).

----------Here Figure 5----------

1.3.3. Polyelectrolyte modified fiberglass membrane characterization

The fiberglass membranes were modified with a polyelectrolyte multilayer by its alternative immersion into a 1 mg·mL^{-1} solution of PEI, PSS, and PHMG. Before modification, each membrane was activated in 1 M NaOH to ensure the negative charge at the membrane surface. The pK_a of SiO_2 – the main component of the membrane (see Fig. SI6 for infra-red spectra) - falls for the range from 2 to 4. Next, after thorough rinsing with distilled water, the membrane was immersed into a solution of branched PEI which served only as a first layer. Following that, the membrane was alternatively placed in a solution of PSS and PHMG until the desired number of layers was obtained. Between each deposition step lasting 5 min, the membrane was always rinsed with distilled water. Membrane modification was followed using infra-red spectroscopy, scanning electron microscopy, and atomic force microscopy. Fig. 6 shows the infra-red spectra recorded for the modified and unmodified membrane in the spectral region where the presence of polyelectrolytes could be followed, this is from 2500 cm^{-1} until 4000 cm^{-1}. After modification three characteristic absorption bands appear with the peak position at 2859 cm^{-1}, 2930 cm$^{-1,}$ and 3214 cm^{-1} that correspond to symmetric and asymmetric CH_2 stretching (all polyelectrolytes) and N-H stretching vibrations (only PEI and PHMG) respectively. Broad peak spanning from 3000 cm^{-1} to 3500 cm^{-1} corresponds to the Si-OH and water adsorbed to the membrane surface.

----------Here Figure 6----------

Next, we have studied the surface characteristics of bare and modified fiberglass membranes using SEM and AFM. Fig. 7A and 7B show membranes before and after modification with PEI(PSS/PHMG)$_3$, respectively. We believe that the seemingly thin-film spanning in between single glass fibers that was present after the modification process (Fig. 7B) is the polyelectrolyte multilayer. As it can be noticed in the inset of Fig. 7B the film is not free from cracks and is decorated with white particles (presumable crystals of the background electrolyte). This is not surprising and most probably originates from the tensions causing film disruption upon drying. With AFM (Fig. 7C, 7D, and 7E) we could reveal the topological changes at the surface of the individual glass fibers already after first – PEI – layer placement. It seems that the first polyelectrolyte layer smoothens the surface of the fibers as the root mean square height (S_q) factor dropped from around 3.3 (+/- 1.9) nm to 1.1 (+/- 0.3) nm. Consecutive layers build with PSS and PHMG increase the surface roughness as the S_q raised to 7.9 (+/- 2.4) nm for PEI(PSS/PHMG)$_3$. Differences in the surface topology can be also inferred directly from the AFM images. We found, that as the number of polyelectrolyte layers increases, the space between single fibers starts to be filled with support (polyelectrolyte multilayer based films) that can be reached by an AFM cantilever. As the size of the polyelectrolytes is significantly lower than the pore sizes within the fiberglass membrane the modification process during LbL processing initially occurs at the surface of individual fibers and in the volume of the membrane. The results obtained for thicker multilayer indicate that the forming polymeric film covers the opening of pores which consequently will limit the diffusivity of polyelectrolyte molecules into the membrane volume (pores will be blocked). At this point, the modification should be happening only at the membrane surface.

----------Here Figure 7----------

1.3.4. Modified fiberglass membrane used as a polarized liquid-liquid interface support

Each polyelectrolyte layer placed at the surface of the fiberglass membrane was characterized with ITV in the presence of four quaternary ammonium cations. We found that the ionic currents flowing through the LLI were affected already after first layer placement, this is PEI. Interestingly, the

ITVs recorded for the membrane modified with PEI (see Fig. SI 7B, 8B, 9B, 10B) gave nonrepeatable signals appearing within the lower potential range of the available potential window. These signals share some characteristics (e.g. signal asymmetry, abrupt drop in the current of the reversed peak) with the ITVs recorded for the PEI or PHMG studied at the non-modified LLI (see section 3.1). Consequently, we have attributed recorded signals to the interfacial adsorption processes of the organic phase anion to the polyelectrolyte species present at the surface of the fiberglass membrane. After second – PSS – and following layers placement the irregular current patterns disappear. Fig. 8B, 8C, 8D, and 8E represent ITVs recorded before (black, solid curves) and after (red, dash-dot curves) fiberglass membrane modification with the PEI(PSS/PHMG)$_3$ being the thickest multilayer studied. These result clearly show that the membrane is still permeable to TMA^+ and TEA^+ although the currents are reduced by 48% and 78%, respectively. For $TPrA^+$ and TBA^+ the ionic currents after modification were not recorded. Assuming the spherical shape of the studied molecules we can calculate their hydrodynamic radius (r) using the Einstein-Stokes equation:

$$D = \frac{k_B T}{6\pi\eta r} \qquad \text{eq. 2}$$

where D is the diffusion coefficient, k_B is the Boltzmann constant ($1.381 \cdot 10^{-23}$ $m^{\cdot 2} kg \cdot s^{-2} \cdot K^{-1}$), T is the temperature (293 K) and η is the dynamic viscosity of water ($8.90 \cdot 10^{-4}$ Pa·s). Calculated r vales for TMA^+, TEA^+, $TPrA^+$ and TBA^+ equal to 0.18 nm, 0.24 nm, 0.35 nm, and 0.38 nm, respectively. With this in mind, and the results shown in Fig. 8A and Fig. SI7 – SI10 we can state that already after first PEI layer placement the membrane is nonpermeable for molecules with the r > 0.38 nm; second PSS layer limits the transfer of molecules with r > 0.35 nm.

----------Here Figure 8----------

The fluctuations in the positive current values recorded after each layer placement (see Fig. 9A) observed especially for TMA^+ and TEA^+, and to a lesser extent for $TPrA^+$, indicate that ions crossing the interface not only experience the physical barrier in a form of pores with narrowing sizes but their transfer across the membrane is also affected electrostatically. This can be confirmed by the

characteristic fluctuating current patterns shown in Fig. 9A. Especially interesting are the zig-zag patterns (Fig. 9B) showing the change in the free Gibbs energy

$$\Delta(\Delta G) = \Delta G_{after\ modification} - \Delta G_{before\ modification} \quad \text{eq. 3}$$

of the ion transfer reaction inferred from Fig. SI7 and SI8 for TMA^+ and TEA^+, respectively. ΔG is expressed as:

$$\Delta G_{i,aq\leftrightarrow org} = -z_i F \Delta_{org}^{aq} \phi_{i,aq\leftrightarrow org} \quad \text{eq. 4}$$

where z is the charge of the ion (z = 1), F is the Faraday constant and $\phi_{i,aq\leftrightarrow org}$ is the Galvani potential of ion transfer taken from the ITVs. For both cations, the additional portion of energy was needed to trigger the interfacial ion transfer when positively charged PHMG was used as the terminating layer, most probably originating from the electrostatic repulsion between positively charged guanidinium groups and positively charged quaternary ammonium cation. When PSS was placed at the surface of the multilayer the change in the free Gibbs energy of the ion transfer was close to zero and slightly positive or slightly negative. For the latter, we can expect the electrostatic attraction that to a small extent facilitates the interfacial transfer. The degree of the change in the free Gibbs energy was significantly more pronounced (one order of magnitude) for TEA^+ as compared with TMA^+. This further confirms that the interfacial transfer across the LLI interface supported with a polyelectrolyte multilayer modified fiberglass membrane is size and charge-dependent.

----------Here Figure 9----------

1.4. Conclusions

In this work the electrified liquid-liquid interface is applied to study fiberglass membranes modified with polyelectrolyte multilayers. In this respect four different quaternary ammonium cations were investigated, *i.e.* TMA^+, TBA^+, $TPrA^+$, and TBA^+. They differ in size and interfacial activety Polyelectrolyte multilayers were formed using PEI, PSS, and PHMG followed by a layer-by-layer assembly at the membrane surface. The multilayer formation was confirmed by using infra-red

spectrometry, scanning electron microscopy, and atomic force microscopy. The ITV data revealed that already after the first layer placement the modified membranes started rejecting the TBA^+ from crossing the interface. The second layer blocked the $TPrA^+$ from crossing the interface. Following polyelectrolyte layers at the membrane surface affected the interfacial transfer of TMA^+ and TEA^+ in an alternative manner showing that the membranes exhibit size and charge sieving properties. The electrified liquid-liquid interface offers a very simple and direct platform for the membrane characterization and visualization of the transmembrane ionic current.

1.5. Acknowledgments

This work was financially supported by the National Science Center (NCN) in Krakow, Poland (Grant no. UMO-2018/31/D/ST4/03259).

1.6. References

[1] J.J. Richardson, M. Björnmalm, F. Caruso, Technology-driven layer-by-layer assembly of nanofilms, Science (80-.). 348 (2015) 411 (1–11). https://doi.org/10.1126/science.aaa2491.

[2] J.J. Richardson, J. Cui, M. Björnmalm, J.A. Braunger, H. Ejima, F. Caruso, Innovation in Layer-by-Layer Assembly, Chem. Rev. 116 (2016) 14828–14867. https://doi.org/10.1021/acs.chemrev.6b00627.

[3] E. Piccinini, C. Bliem, C. Reiner-Rozman, F. Battaglini, O. Azzaroni, W. Knoll, Enzyme-polyelectrolyte multilayer assemblies on reduced graphene oxide field-effect transistors for biosensing applications, Biosens. Bioelectron. 92 (2017) 661–667. https://doi.org/10.1016/j.bios.2016.10.035.

[4] M.L. Cortez, A.L. Cukierman, F. Battaglini, Surfactant presence in a multilayer polyelectrolyte-enzyme system improves its catalytic response, Electrochem. Commun. 11 (2009) 990–993. https://doi.org/10.1016/j.elecom.2009.02.041.

[5] C. Schüler, F. Caruso, Preparation of enzyme multilayers on colloids for biocatalysis,

Macromol. Rapid Commun. 21 (2000) 750–753. https://doi.org/10.1002/1521-3927(20000701)21:11<750::AID-MARC750>3.0.CO;2-3.

[6] N. Dizge, R. Epsztein, W. Cheng, C.J. Porter, M. Elimelech, Biocatalytic and salt selective multilayer polyelectrolyte nanofiltration membrane, J. Memb. Sci. 549 (2018) 357–365. https://doi.org/10.1016/j.memsci.2017.12.026.

[7] D. Mertz, C. Vogt, J. Hemmerlé, C. Debry, J.C. Voegel, P. Schaaf, P. Lavalle, Tailored design of mechanically sensitive biocatalytic assemblies based on polyelectrolyte multilayers, J. Mater. Chem. 21 (2011) 8324–8331. https://doi.org/10.1039/c0jm03496g.

[8] K. Katagiri, R. Hamasaki, K. Ariga, J. Kikuchi, Layer-by-Layer Self-Assembling of Liposomal Nanohybrid “Cerasome” on Substrates, Langmuir. 132 (2002) 6709–6711.

[9] E. Diamanti, L. Cuellar, D. Gregurec, S.E. Moya, E. Donath, Role of Hydrogen Bonding and Polyanion Composition in the Formation of Lipid Bilayers on Top of Polyelectrolyte Multilayers, Langmuir. 31 (2015) 8623–8632. https://doi.org/10.1021/acs.langmuir.5b01731.

[10] S. Moya, E. Donath, G.B. Sukhorukov, M. Auch, H. Baumler, H. Lichtenfeld, H. Mohwald, Lipid coating on polyelectrolyte surface modified colloidal particles and polyelectrolyte capsules, Macromolecules. 33 (2000) 4538–4544. https://doi.org/10.1021/ma9914974.

[11] R. Kügler, W. Knoll, Polyelectrolyte-supported lipid membranes, Bioelectrochemistry. 56 (2002) 175–178. https://doi.org/10.1016/S1567-5394(02)00031-2.

[12] L. Poltorak, M.L. Verheijden, D. Bosma, P. Jonkheijm, L.C.P.M. de Smet, E.J.R. Sudhölter, BBA - Biomembranes Lipid bilayers cushioned with polyelectrolyte-based films on doped silicon surfaces, BBA - Biomembr. 1860 (2018) 2669–2680. https://doi.org/10.1016/j.bbamem.2018.09.018.

[13] A.G. Skirtach, A.M. Yashchenok, H. Möhwald, Encapsulation, release and applications of LbL polyelectrolyte multilayer capsules, Chem. Commun. 47 (2011) 12736–12746.

https://doi.org/10.1039/c1cc13453a.

[14] L.L. Del Mercato, M.M. Ferraro, F. Baldassarre, S. Mancarella, V. Greco, R. Rinaldi, S. Leporatti, Biological applications of LbL multilayer capsules: From drug delivery to sensing, Adv. Colloid Interface Sci. 207 (2014) 139–154. https://doi.org/10.1016/j.cis.2014.02.014.

[15] E.M. Shchukina, D.G. Shchukin, LbL coated microcapsules for delivering lipid-based drugs, Adv. Drug Deliv. Rev. 63 (2011) 837–846. https://doi.org/10.1016/j.addr.2011.03.009.

[16] L. Paltrinieri, M. Wang, S. Sachdeva, N.A.M. Besseling, E.J.R. Sudhölter, L.C.P.M. De Smet, Fe3O4 nanoparticles coated with a guanidinium-functionalized polyelectrolyte extend the pH range for phosphate binding, J. Mater. Chem. A. 5 (2017) 18476–18485. https://doi.org/10.1039/c7ta04054g.

[17] Z. Zhao, S. Shi, H. Cao, Y. Li, B. Van der Bruggen, Layer-by-layer assembly of anion exchange membrane by electrodeposition of polyelectrolytes for improved antifouling performance, J. Memb. Sci. 558 (2018) 1–8. https://doi.org/10.1016/j.memsci.2018.04.035.

[18] H. Gao, B. Zhang, X. Tong, Y. Chen, Monovalent-anion selective and antifouling polyelectrolytes multilayer anion exchange membrane for reverse electrodialysis, J. Memb. Sci. 567 (2018) 68–75. https://doi.org/10.1016/j.memsci.2018.09.035.

[19] X. Zhu, D. Jańczewski, S.S.C. Lee, S.L.M. Teo, G.J. Vancso, Cross-linked polyelectrolyte multilayers for marine antifouling applications, ACS Appl. Mater. Interfaces. 5 (2013) 5961–5968. https://doi.org/10.1021/am4015549.

[20] S. Abdu, M.C. Martí-Calatayud, J.E. Wong, M. García-Gabaldón, M. Wessling, Layer-by-layer modification of cation exchange membranes controls ion selectivity and water splitting, ACS Appl. Mater. Interfaces. 6 (2014) 1843–1854. https://doi.org/10.1021/am4048317.

[21] H. Deng, Z. Wang, W. Zhang, B. Hu, S. Zhang, Preparation and monovalent selective properties of multilayer polyelectrolyte modified cation-exchange membranes, J. Appl.

Polym. Sci. 132 (2015) 1–7. https://doi.org/10.1002/app.41488.

[22] W. Jin, A. Toutianoush, B. Tieke, Size- and charge-selective transport of aromatic compounds across polyelectrolyte multilayer membranes, Appl. Surf. Sci. 246 (2005) 444–450. https://doi.org/10.1016/j.apsusc.2004.11.067.

[23] S.U. Hong, R. Malaisamy, M.L. Bruening, Optimization of flux and selectivity in Cl-/SO42- separations with multilayer polyelectrolyte membranes, J. Memb. Sci. 283 (2006) 366–372. https://doi.org/10.1016/j.memsci.2006.07.007.

[24] C.J. Slevin, A. Malkia, P. Liljeroth, M. Toiminen, Kyosti Kontturi, Electrochemical Characterization of Polyelectrolyte Multilayers Deposited at Liquid - Liquid Interfaces, Langmuir. 19 (2003) 1287–1294.

[25] L. Paltrinieri, L. Poltorak, L. Chu, T. Puts, W. van Baak, E.J.R. Sudhölter, L.C.P.M. de Smet, Hybrid polyelectrolyte-anion exchange membrane and its interaction with phosphate, React. Funct. Polym. 133 (2018) 126–135. https://doi.org/10.1016/j.reactfunctpolym.2018.10.005.

[26] L. Paltrinieri, K. Remmen, B. Müller, L. Chu, J. Köser, T. Wintgens, M. Wessling, L.C.P.M. de Smet, E.J.R. Sudhölter, Improved phosphoric acid recovery from sewage sludge ash using layer-by-layer modified membranes, J. Memb. Sci. 587 (2019) 117162. https://doi.org/10.1016/j.memsci.2019.06.002.

[27] F. Reymond, D. Fermin, H.J. Lee, H.H. Girault, Electrochemistry at liquid/liquid interfaces: methodology and potential applications, Electochim. Acta. 45 (2000) 2647–2662. http://linkinghub.elsevier.com/retrieve/pii/S0013468600003431.

[28] Z. Samec, Electrochemistry at the interface between two immiscible electrolyte solutions (IUPAC technical report), Pure Appl. Chem. 76 (2004) 2147–2180.

[29] L. Poltorak, A. Gamero-Quijano, G. Herzog, A. Walcarius, Decorating soft electrified interfaces: From molecular assemblies to nano-objects, Appl. Mater. Today. 9 (2017) 533–

550. https://doi.org/10.1016/j.apmt.2017.10.001.

[30] H.A. Santos, S. Carlsson, L. Murtomäki, K. Kontturi, Effect of gramicidin on phospholipid-modified monolayers and on ion transfer at a liquid-liquid interface., Chemphyschem. 8 (2007) 913–920. https://doi.org/10.1002/cphc.200600767.

[31] J.A. Manzanares, R.M. Allen, K. Kontturi, Enhanced ion transfer rate due to the presence of zwitterionic phospholipid monolayers at the ITIES, J. Electroanal. Chem. 483 (2000) 188–196. https://doi.org/10.1016/S0022-0728(00)00032-2.

[32] S.G. Booth, R. a W. Dryfe, Assembly of Nanoscale Objects at the Liquid/Liquid Interface, J. Phys. Chem. C. 119 (2015) 23295–23309. https://doi.org/10.1021/acs.jpcc.5b07733.

[33] S. Senthilkumar, R.A.W. Dryfe, R. Saraswathi, Size-selective voltammetry: modification of the interface between two immiscible electrolyte solutions by zeolite Y, Langmuir. 23 (2007) 3455–3461. http://www.ncbi.nlm.nih.gov/pubmed/17279783.

[34] L. Poltorak, K. Morakchi, G. Herzog, A. Walcarius, Electrochemical characterization of liquid-liquid micro-interfaces modified with mesoporous silica, Electrochim. Acta. 179 (2015) 9–15. https://doi.org/10.1016/j.electacta.2015.01.129.

[35] R.A.W. Dryfe, S.M. Holmes, Zeolitic rectification of electrochemical ion transfer, J. Electroanal. Chem. 483 (2000) 144–149. http://linkinghub.elsevier.com/retrieve/pii/S0022072899005069.

[36] L. Xie, X. Huang, B. Su, Portable Sensor for the Detection of Choline and Its Derivatives Based on Silica Isoporous Membrane and Gellified Nanointerfaces, ACS Sensors. 2 (2017) 803–809. https://doi.org/10.1021/acssensors.7b00166.

[37] M.D. Scanlon, J. Strutwolf, A. Blake, D. Iacopino, A.J. Quinn, D.W.M. Arrigan, Ion-transfer electrochemistry at arrays of nanointerfaces between immiscible electrolyte solutions confined within silicon nitride nanopore membranes, Anal. Chem. 82 (2010) 6115–6123.

https://doi.org/10.1021/ac1008282.

[38] Y.H. Lanyon, G. De Marzi, Y.E. Watson, A.J. Quinn, J.P. Gleeson, G. Redmond, D.W.M. Arrigan, Fabrication of nanopore array electrodes by focused ion beam milling, Anal. Chem. 79 (2007) 3048–3055. https://doi.org/10.1021/ac061878x.

[39] M. Rimboud, R.D. Hart, T. Becker, D.W.M. Arrigan, Electrochemical behaviour and voltammetric sensitivity at arrays of nanoscale interfaces between immiscible liquids, Analyst. 136 (2011) 4674–4681. https://doi.org/10.1039/c1an15509a.

[40] L. Poltorak, I. Eggink, M. Hoitink, M. De Puit, E.J.R.E.J.R. Sudholter, M. De Puit, Electrified soft interface as a selective sensor for cocaine detection in street samples, Anal. Chem. 90 (2018) 8–13. https://doi.org/10.1021/acs.analchem.8b00916.

[41] F. Roghmans, E. Evdochenko, F. Stockmeier, S. Schneider, A. Smailji, R. Tiwari, A. Mikosch, E. Karatay, A. Kühne, A. Walther, A. Mani, M. Wessling, 2D Patterned Ion-Exchange Membranes Induce Electroconvection, Adv. Mater. Interfaces. 6 (2019) 1–11. https://doi.org/10.1002/admi.201801309.

[42] B. Kralj, R. a. W. Dryfe, Membrane voltammetry: The interface between two immiscible electrolyte solutions, Phys. Chem. Chem. Phys. 3 (2001) 5274–5282. https://doi.org/10.1039/b107463f.

[43] X. Huang, L. Xie, X. Lin, B. Su, Permselective Ion Transport Across the Nanoscopic Liquid/Liquid Interface Array, Anal. Chem. 88 (2016) 6563–6569. https://doi.org/10.1021/acs.analchem.6b01383.

[44] L. Poltorak, G.G. Herzog, A. Walcarius, Electrochemically assisted generation of silica deposits using a surfactant template at liquid/liquid microinterfaces, Langmuir. 30 (2014) 11453–11463. https://doi.org/10.1021/la501938g.

[45] L. Chu, M. Bus, A. V Korobko, N.A.M. Besseling, Calibrating lateral displacement sensitivity of

AFM by stick-slip on stiff, amorphous surfaces, Ultramicroscopy. 205 (2019) 1–4. https://doi.org/10.1016/j.ultramic.2019.05.012.

[46] H.J. Butt, M. Jaschke, Calculation of thermal noise in atomic force microscopy, Nanotechnology. 6 (1995) 1–7.

[47] C. Tabor, H. Tabor, Polyamines, 2011. http://medcontent.metapress.com/index/A65RM03P4874243N.pdf%5Cnhttp://www.annualreviews.org/doi/pdf/10.1146/annurev.bi.53.070184.003533.

[48] G.M. Olmedo, L. Cerioni, M. Sepulveda, J. Ramallo, V.A. Rapisarda, S.I. Volentini, Polyhexamethylene guanidine as a fungicide, disinfectant and wound protector in lemons challenged with Penicillium digitatum, Food Microbiol. 76 (2018) 128–134. https://doi.org/10.1016/j.fm.2018.03.018.

[49] S.R. Lewis, S. Datta, M. Gui, E.L. Coker, F.E. Huggins, S. Daunert, L. Bachas, D. Bhattacharyya, Reactive nanostructured membranes for water purification, Proc. Natl. Acad. Sci. 108 (2011) 8577–8582. https://doi.org/10.1073/pnas.1101144108.

[50] G. Herzog, P. Eichelmann-Daly, D.W.M. Arrigan, Electrochemical behaviour of denatured haemoglobin at the liquid|liquid interface, Electrochem. Commun. 12 (2010) 335–337. https://doi.org/10.1016/j.elecom.2009.12.020.

[51] G. Herzog, W. Moujahid, J. Strutwolf, D.W.M. Arrigan, Interactions of proteins with small ionised molecules: Electrochemical adsorption and facilitated ion transfer voltammetry of haemoglobin at the liquid/liquid interface, Analyst. 134 (2009) 1608–1613. https://doi.org/10.1039/b905441n.

[52] G. Herzog, V. Kam, D.W.M. Arrigan, Electrochemical behaviour of haemoglobin at the liquid/liquid interface, Electrochim. Acta. 53 (2008) 7204–7209. https://doi.org/10.1016/j.electacta.2008.04.072.

[53] L. Poltorak, N. van der Meijden, S. Oonk, E.J.R. Sudhölter, M. de Puit, Acid phosphatase behaviour at an electrified soft junction and its interfacial co-deposition with silica, Electrochem. Commun. 94 (2018) 27–30. https://doi.org/10.1016/j.elecom.2018.07.022.

[54] J.S. Riva, C.I. Cámara, A. V. Juarez, L.M. Yudi, Electrochemical behaviour of cationic polyelectrolytes at a polarized liquid/liquid interface, J. Appl. Electrochem. 44 (2014) 1381–1392. https://doi.org/10.1007/s10800-014-0747-2.

[55] S. Ulmeanu, H.J. Lee, H.H. Girault, Voltammetric characterisation of polyelectrolyte adsorption/transfer at the water/1,2-DCE interface, Electrochem. Commun. 3 (2001) 539–543. https://doi.org/10.1016/S1388-2481(01)00209-0.

[56] R.A. Hartvig, M.A. Méndez, M. Van De Weert, L. Jorgensen, J. Østergaard, H.H. Girault, H. Jensen, Interfacial complexes between a protein and lipophilic ions at an oil-water interface, Anal. Chem. 82 (2010) 7699–7705. https://doi.org/10.1021/ac101528r.

[57] Z. Cao, P.I. Gordiichuk, K. Loos, E.J.R. Sudhölter, L.C.P.M. de Smet, The effect of guanidinium functionalization on the structural properties and anion affinity of polyelectrolyte multilayers, Soft Matter. 12 (2016) 1496–1505. https://doi.org/10.1039/C5SM01655J.

[58] S. Liu, Q. Li, Y. Shao, Electrochemistry at micro- and nanoscopic liquid/liquid interfaces., Chem. Soc. Rev. 40 (2011) 2236–53. https://doi.org/10.1039/c0cs00168f.

[59] T. Hinoue, E. Ikeda, S. Watariguchi, Y. Kibune, Thermal modulation voltammetry with laser heating at an aqueous|nitrobenzene solution microinterface: determination of the standard entropy changes of transfer for tetraalkylammonium ions., Anal. Chem. 79 (2007) 291–8. https://doi.org/10.1021/ac061315l.

Captions

Figure 1. A – the classical glass cell used to support macroscopic LLI; B – the glass cell used to study the modified and unmodified fiberglass membrane supported LLI; C – the optical microscopy photo of the unmodified glass fiber membrane; D – schematic representation of the fiberglass membrane modified with polyelectrolyte multilayer. 1 and 2 are the organic phase and the aqueous phase counter electrodes, respectively. 3 and 4 are the Ag/AgCl reference electrodes placed in both phases each. PEI - poly(ethyleneimine); PSS - polystyrene sulfonate; PHMG - polyhexamethylene guanidine.

Figure 2. Ion transfer voltammograms recorded for **A –** 50 μg/mL PHMG (aqueous phase: 10 mM NaCl); **B –** 50 μg/mL PEI (aqueous phase: 10 mM HCl in 10 mM NaCl); **C –** 50 μg/mL PSS (aqueous phase: 10 mM NaCl); D – blank voltammogram (aqueous phase: 10 mM NaCl). The organic phase was 5 mM BTPPATPBCl dissolved in 1,2-dichloroethane. Scan rate was 10 $mV \cdot s^{-1}$. Structures of an uncharged polyelectrolyte are placed on the right from the corresponding voltammogram.

Figure 3. A – the ion transfer voltammograms recorded in cell II, for PHMG = 20 μg/mL, for the 2^{nd} (red, dot-dash curve) and 100^{th} cycle (black, solid curve). **B** – forward signal peak currents normalized values recorded over 100 consecutive scans for pH equal to 5.0; 7.4; 10.0 and 12.0 (for the symbols refer to the legend available in the inset).

Figure 4. A – ion transfer voltammograms recorded at the LLI supported with the unmodified fiberglass membrane in the presence (red curve) and the absence (black curve) of 150 μM TMA^+Cl^- initially dissolved in the aqueous phase. The scan rate was 20 $mV \cdot s^{-1}$. **B** – schematic representation of the fiberglass membrane supporting LLI with the hemispherical diffusion zones established on the pores ingress from the aqueous and the organic phase side.

Figure 5. Series of ion transfer voltammograms (and corresponding calibration curves – right column) recorded for a family of quaternary ammonium cations at the liquid-liquid interface supported with unmodified glass fiber membrane. The studied concentration equal to 50; 100; 150 and 200 μM. **A** and **B** – TMA^+Cl^-; **C** and **D** – TEA^+Cl^-; **E** and **F** – $TPrA^+Cl^-$; **G** and **H** – TBA^+Cl^-. The scan rate was 20 $mV \cdot s^{-1}$.

Figure 6. Infra-red spectra recorded for unmodified (black, bottom curve) and polyelectrolyte multilayer modified (red, upper curve) membrane. Absorption bands of interest are indicated with arrows. Polyelectrolyte layer thickness – $PEI(PSS\text{-}PHMG)_5$.

Figure 7. A and **B** are the SEM micrographics recorded for the fiberglass membrane before and after modification with $PEI(PSS/PHMG)_3$ multilayer, respectively. Insets show the magnification. AFM topological images showing unmodified glass fibers (C), glass fibers modified with $PEI(PSS/PHMG)_1$ (D), and $PEI(PSS/PHMG)_3$ (E) are given as the bottom panel. F is the root mean square height calculated as an average from three positions as a function of polyelectrolyte layer thickness. The number of layers equal to zero represents the unmodified fiberglass membrane.

Figure 8. A – schematic and simplified representation of the polyelectrolyte multilayer growing at the surface of the fiberglass membrane. **B, C, D**, and **E** are the ITVs recorded before (solid, black line) and after (red, dash-dot lines) fiberglass membrane modification with $PEI(PSS/PHMG)_3$ for TMA^+, TEA^+, $TPrA^+$, and TBA^+ respectively. The concentration of each quaternary ammonium cation was set to 200 μM. Scan rate = 20 $mV \cdot s^{-1}$.

Figure 9. A – Positive peak current values for four studied quaternary ammonium cations (see the corresponding legend) as a function of the layer thickness. Prepared based on Fig. SI6 – SI9. **B** – Change in the free Gibbs energy (eq. 3) of the ion transfer reaction for TMA^+ and TEA^+ as a function of the layer thickness. Prepared based on Fig. SI6 and SI7.

Figures

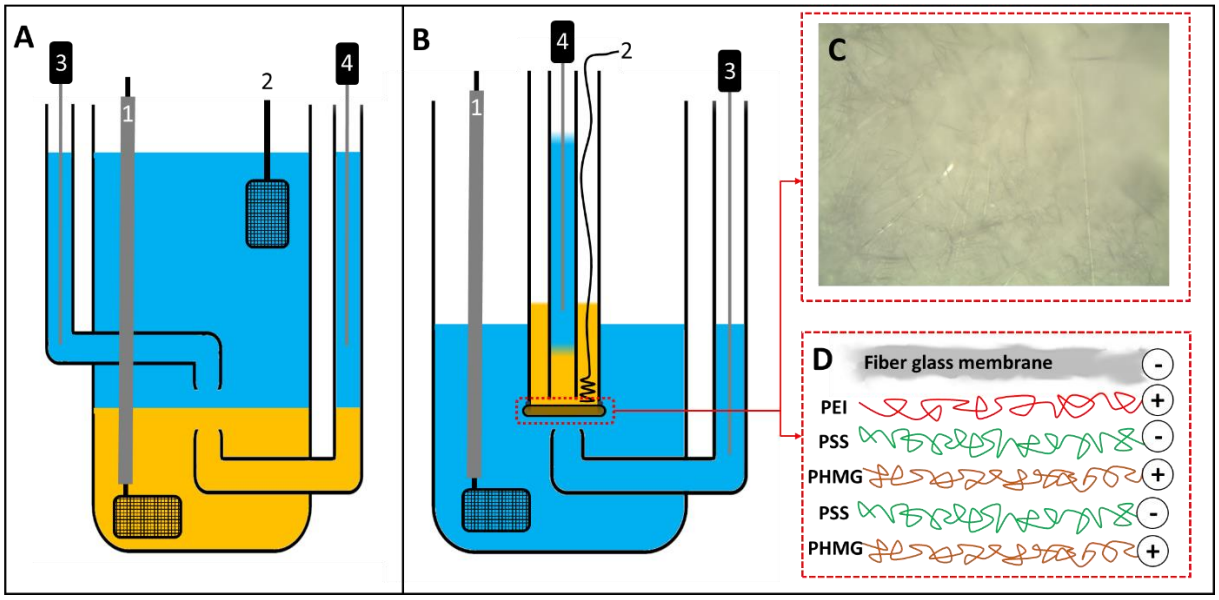

Figure 1.

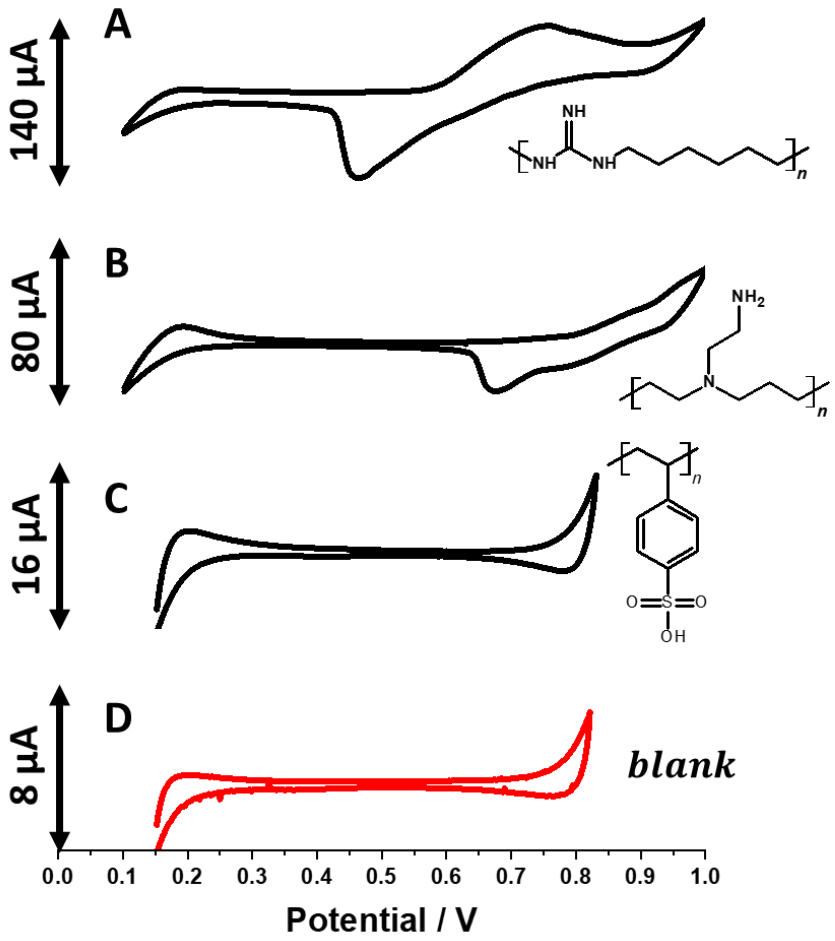
A
140 µA
NH
NH
NH
n
B
80 µA
NH2
N
n
C
16 µA
n
O
S
O
OH
D
8 µA
blank
0.0
0.1
0.2
0.3
0.4
0.5
0.6
0.7
0.8
0.9
1.0
Potential / V

Figure 2.

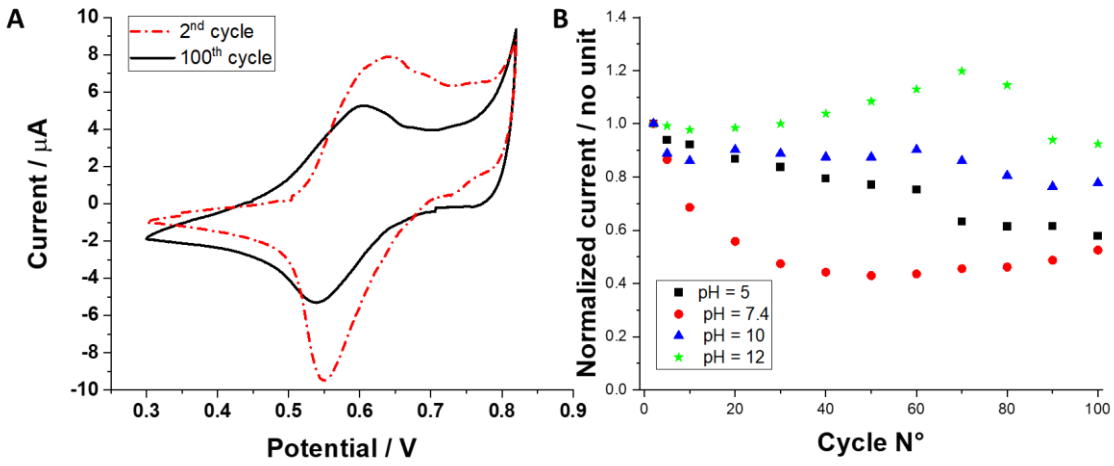
A
2nd cycle
100th cycle
Current / µA
Potential / V
B
Normalized current / no unit
pH = 5
pH = 7.4
pH = 10
pH = 12
Cycle N°

Figure 3.

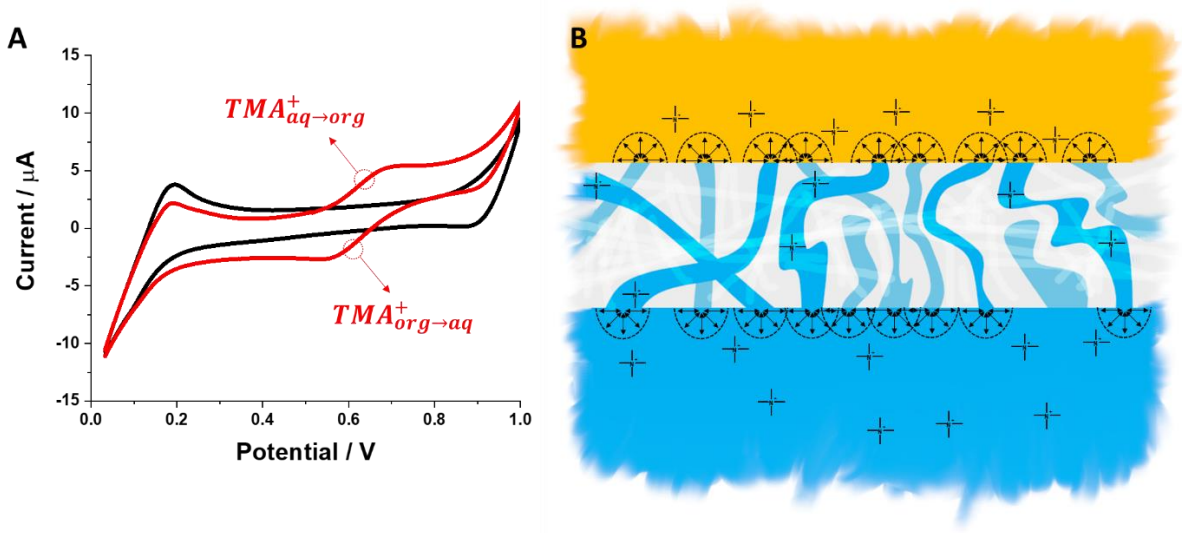
A
B
Current / μA
Potential / V
15
10
5
0
-5
-10
-15
0.0
0.2
0.4
0.6
0.8
1.0
$TMA^{+}_{aq\rightarrow org}$
$TMA^{+}_{org\rightarrow aq}$

Figure 4.

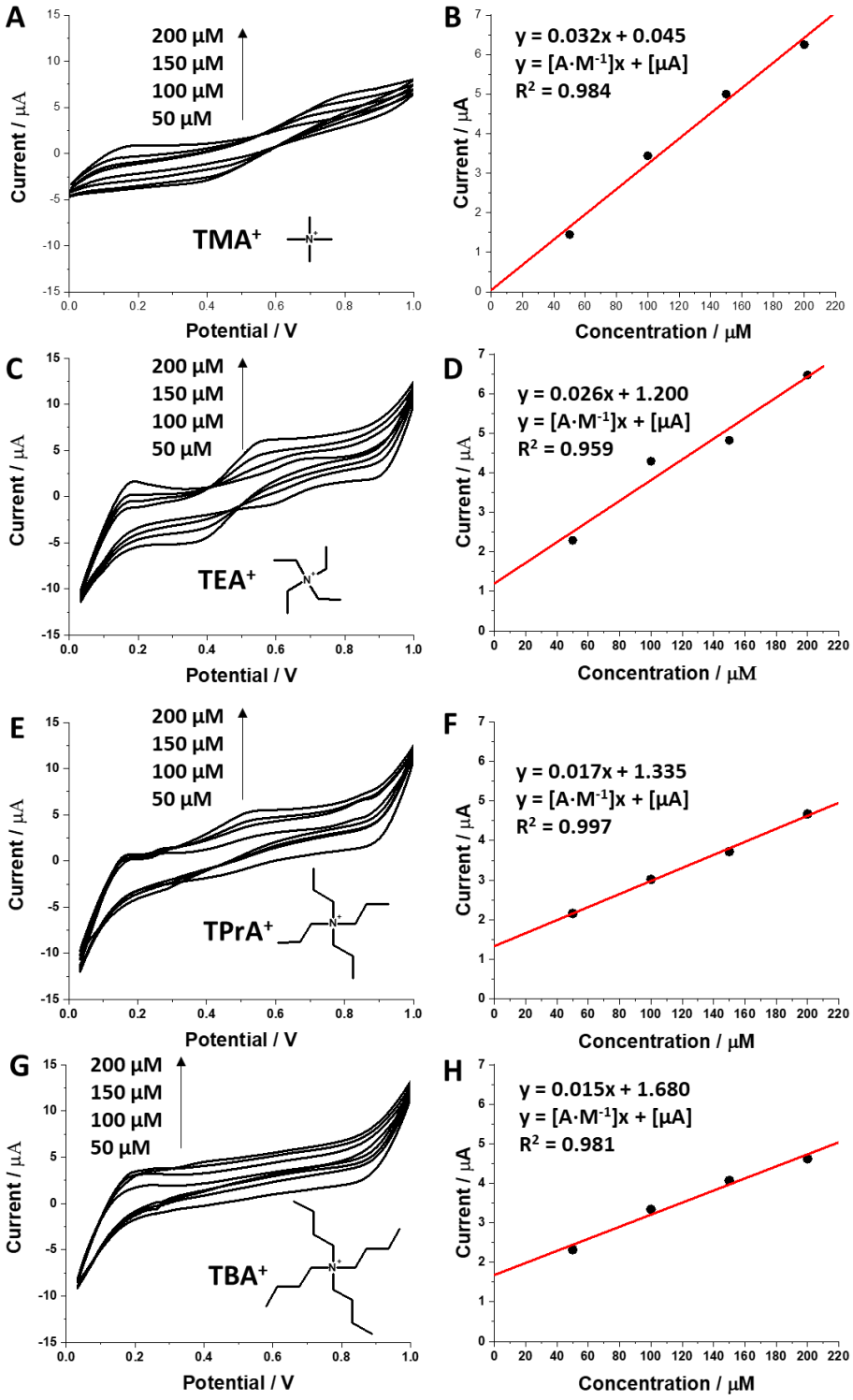
A
200 µM
150 µM
100 µM
50 µM
TMA+
Current / µA
Potential / V
B
y = 0.032x + 0.045
y = [A·M-1]x + [µA]
R2 = 0.984
Current / µA
Concentration / µM
C
200 µM
150 µM
100 µM
50 µM
TEA+
Current / µA
Potential / V
D
y = 0.026x + 1.200
y = [A·M-1]x + [µA]
R2 = 0.959
Current / µA
Concentration / µM
E
200 µM
150 µM
100 µM
50 µM
TPrA+
Current / µA
Potential / V
F
y = 0.017x + 1.335
y = [A·M-1]x + [µA]
R2 = 0.997
Current / µA
Concentration / µM
G
200 µM
150 µM
100 µM
50 µM
TBA+
Current / µA
Potential / V
H
y = 0.015x + 1.680
y = [A·M-1]x + [µA]
R2 = 0.981
Current / µA
Concentration / µM

Figure 5.

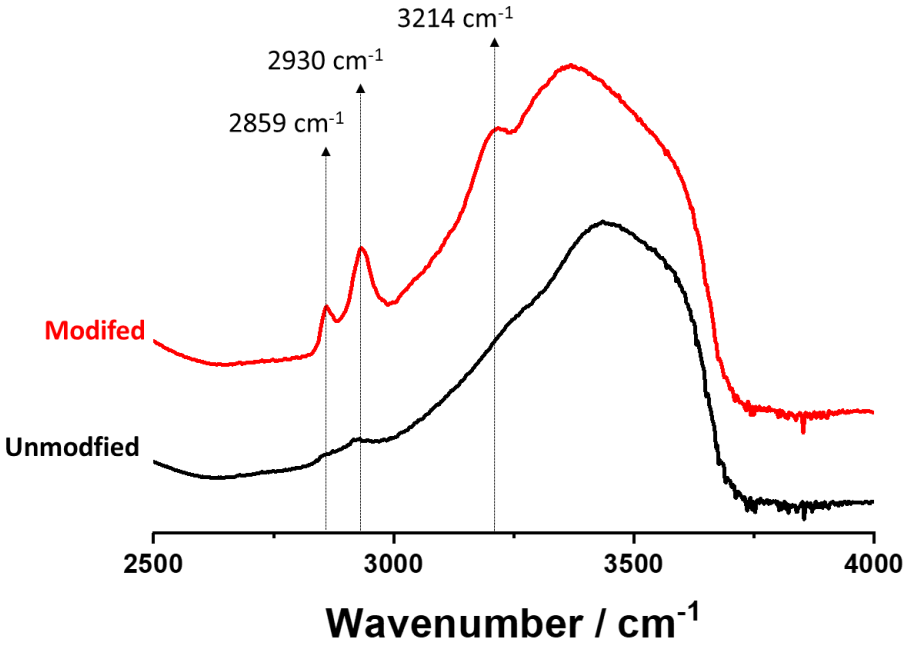
3214 cm-1
2930 cm-1
2859 cm-1
Modifed
Unmodfied
2500
3000
3500
4000
Wavenumber / cm-1

Figure 6.

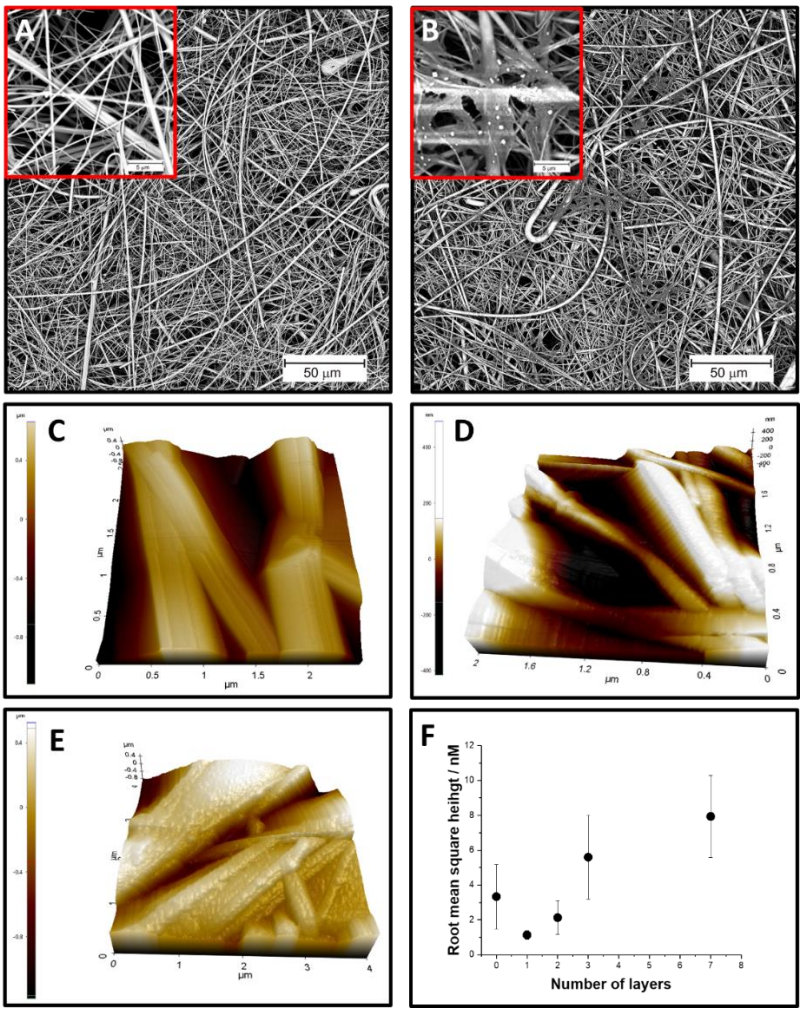
A
B
50 µm
50 µm
C
D
E
F
Root mean square heihgt / nM
Number of layers

Figure 7.

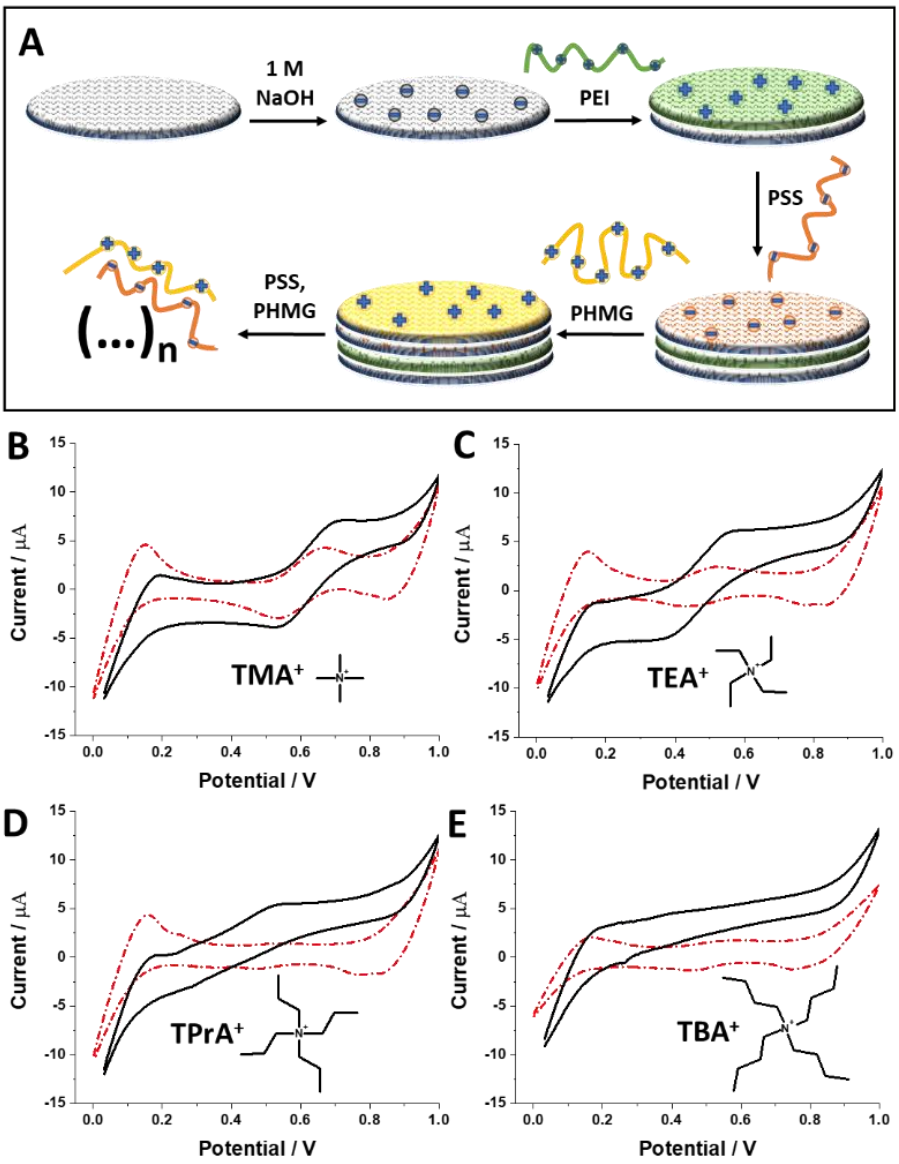
A
1 M
NaOH
PEI
PSS
PSS,
PHMG
PHMG
(...)n
B
C
D
E
Current / µA
Potential / V
TMA+
TEA+
TPrA+
TBA+

Figure 8.

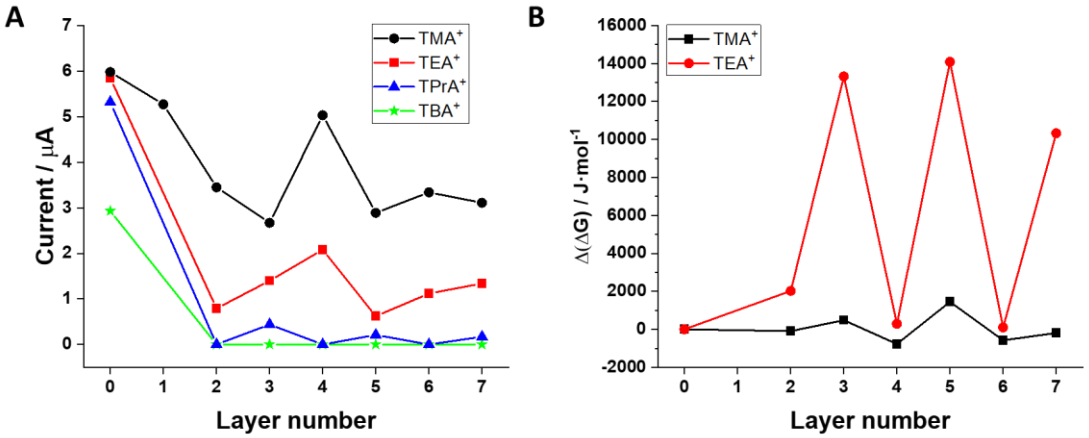
A
Current / μA
Layer number
TMA+
TEA+
TPrA+
TBA+
B
Δ(ΔG) / J·mol-1
Layer number
TMA+
TEA+

Figure 9.